# Macroscopic Polymer Analogues

**G. BEAUCAGE, S. SUKUMARAN, S. RANE, D. J. KOHLS**

Polymer Research Center and Department of Materials Science and Engineering, P.O. Box 210012, University of Cincinnati, Cincinnati, Ohio 45221-0012

*Received 20 April 1998; revised 29 July 1998; accepted 31 July 1998*

**ABSTRACT:** Disordered fiber mats made of glass microfibers (GMF) were studied using small-angle light scattering (SALS), ultrasmall-angle X-ray scattering (USAXS), SEM, and optical microscopy. The morphological scaling of these materials in the micron scale was very similar to that of polymers in the nanometer scale. In some fiber mats, such as GMF, the structure is randomized at the time of formation, leading to a statistical analogy with the thermal randomization that occurs in nanometer-scale, high polymers. Analogues for the coil radius-of-gyration, persistence unit, and scaling regimes exist in such fiber mats and may be a useful feature both for modeling thermally equilibrated polymeric systems, as well as furthering the understanding of the physical properties of fiber mats through analogy with the theoretical understanding of thermally equilibrated polymeric systems. © 1998 John Wiley & Sons, Inc. J Polym Sci B: Polym Phys 36: 3147–3154, 1998

**Keywords:** glass microfiber; scattering; polymer; nonwoven fabrics; polymer analogue

## INTRODUCTION

Some disordered fiber mats represent an interesting analog to nanometer-scale linear polymeric systems. These fibrous materials are, of course, not subject to thermal equilibrium in the determination of structure. However, they are statistics-based materials with fixed stochastic-scaling regimes associated with their formation process. This article focuses on silica glass microfibers that are produced as disordered fiber mats in an extrusion process where a web of micron-diameter fibers are spun from a melt and extruded in a rapid process into a sheet of disordered fibers. Fiber diameters are on the micron scale, while fiber lengths are on the millimeter scale, offering a wide scaling regime covering many decades in size. Whereas linear polymeric systems display nano-scale structure with a scaling regime generally on the 10 to 300 Å scale, glass microfibers (GMF) display a characteristic scaling regime on the 1 to 1000 micron scale. Scaling regimes for linear organic polymers are observed using small-angle neutron or X-ray scattering with wavelengths on the Angstrom scale.[1–3] Fiber scaling can be observed using light scattering if careful attention is paid to reduction of the scattering contrast through the use of an index matching fluid that does not alter the micron-scale morphology.

In linear, nanometer-scale polymers several scaling regimes are known both from theory and experiment.[1–6] The Gaussian state represents a random distribution that ignores chain–chain repulsion due to volumetric exclusion through a balance between entropic randomization and enthalpic attraction.[4–7] For the Gaussian state, the mass-fractal dimension, $d_f$, is 2, i.e., coil mass $\alpha$ $z$ $\alpha$ $R^2$, where $z$ is the number of Kuhn steps in a chain of average size $R$. In the absence of such thermodynamic attraction between chain segments, i.e., in good solvents, the coil scaling follows a mass-fractal dimension of 5/3 rather than 2, Mass $\alpha$ $R^{5/3}$. Because GMF fibers display essentially no attractive or repulsive interaction, it is expected that these systems could follow an

*Correspondence to:* G. Beaucage

Journal of Polymer Science: Part B: Polymer Physics, Vol. 36, 3147–3154 (1998)
 CCC 0887-6266/98/173147-08

analogy for good-solvent scaling for repulsive/nonoverlapping coils in a most random state. (This expected good-solvent scaling might be overcome by some type of bonding between fibers, e.g., so-called spun-bonded materials.)

In addition to a scaling regime, three other morphological features define a typical nanometer-scale, linear polymer. At the largest size is the radius of gyration for a single polymer coil, which is directly related to the end-to-end distance by familiar relationships. At the smallest scale, a linear organic polymer is expected to display a persistence regime where scaling goes to 1D for a rod-like persistence unit. The persistence unit is generally described by a Kuhn-step length, $K$, and a diameter, $D$. GMF might also be expected to display both of these features in the light-scattering regime. In these macroscopic analogues, the absence of local structure based on chemical bonds is expected to lead to low degrees of local persistence, and a small persistence length relative to the fiber diameter.

The formation process of disordered fiber mats, such as GMF, has a degree of global asymmetry because these materials are generally produced in a continuous process in the form of a sheet. For these sheets, a high degree of orientation is expected in the cross-section. This orientation can be quantified using SALS through adoption of the Hermans Orientation function,[8] as discussed below, and through sector averaging of 2D SALS data.

A combination of microscopy and small-angle scattering can be used to describe these statistical features of disordered fiber mats if a wide range of scattering vector, $q$, is available and if global scattering functions are used. Such a global function, the unified equation,[9–11] can be used to fit the scattering data from such mass-fractal systems displaying scaling transitions. The unified function can describe scattering with multiple scaling transitions and arbitrary mass-fractal dimensions.[9–12] It has recently been adapted to dealing with polymer chain structure.[12] Typically, nanometer-scale polymers display a scaling regime characteristic of the thermal state of the coil at low $q$ followed by a persistence regime of $-1$ slope (in a log intensity vs. log $q$ plot) reflecting local, linear persistence units. The GMF data, discussed below, does not show a clear persistence regime reflecting extremely short persistence units of the order of the diameter of a fiber. Such a situation can occur when the aspect ratio between the persistence length, $K/2$, and the fiber diameter is less than about 2.[3] For such systems the Kuhn unit and fiber diameter, $D$, are grouped into a single fitting parameter reflecting local chain structure, the local radius of gyration, $R_{g1}^2 = K^2/12 + D^2/8$. This size-scale is reflected in a Guinier regime at high $q$ followed by a Porod regime, which accounts for the surface scattering from the fibers. The complete scattering curve from such fibers can be fit using the unified approach and four parameters, the fiber contrast/concentration based Guinier term, $G_1$, the fiber diameter, $D$, fiber Kuhn-step length, $K$, and the number of Kuhn units in an average fiber, $z$. GMF fiber mats display two power-law regimes, and two Guinier regimes accounted for in the unified approach by two levels of structure, level 1 for the local structure and level 2 for the coil structure,

$$I(q) = \{G_2 e^{-q^2 R_{g2}^2/3} + B_2 e^{-q^2 R_{g1}^2/3} (q_2^*)^{-d_f}\} + \{G_1 e^{-q^2 R_{g1}^2/3} + B_1 (q_1^*)^{-4}\} \quad (1)$$

where the six parameters of eq. (1) can all be calculated from $G_1$, $D$, $K$, and $z$.[9–12] For the parameters of eq. (1)

$$G_2 = z\ G_1,\ R_{g2}^2 = \frac{K^2 z^{2/d_f}}{(1 + 2/d_f)(2 + 2/d_f)}$$

where $d_f = 5/3$ for a self-avoiding walk,

$$B_2 = \frac{d_f G_2}{R_{g2}^{d_f}} \Gamma(d_f/2),\ q_i^* = \frac{q}{[erf(qR_{gi}/\sqrt{6})]^3},$$

$$R_{g1}^2 = K^2/12 + D^2/8,$$

and $B_1 = 32\ G_1/(KD^3)$ from Porod's Law for a cylinder with surface area only on the sides.[13] The number of Kuhn steps in an average fiber, $z$, is a first-order moment of the distribution if it is calculated from, $G_2 = z\ G_1$, because the Guinier prefactor $G_2$ is directly proportional to the number of mer units.[9–12]

## EXPERIMENTAL

Typically, contrast differences for light scattering are much higher than for X-ray or neutron scattering, necessitating more complicated scattering functions based on Mie Theory. Under conditions of low contrast, the Rayleigh–Gans approximation greatly simplifies scattering laws and is the basis of such common SAXS and SANS laws as Guinier's law and Porod and power-law scaling

laws, as well as the unified equation discussed above. To use the Rayleigh–Gans approximation to analyze SALS data for GMF, the contrast for the system must be significantly reduced. This can easily be accomplished through the use of an index-matching liquid in which the sample is immersed. For silica glass, benzyl alcohol is close in index of refraction (1.538 for benzyl alcohol and 1.5 for silica glass). The basic assumption in the use of a contrast-matching solvent is that the structure is not perturbed by the solvent. This can be verified by consideration of the bulk size and shape of the sample, through the use of several different solvents, and by microscopic observation.

SALS experiments were performed using a 10-mW HeNe laser at 0.6328 $\mu$m wavelength with a 1-mm beam collimated using two 0.5-mm pinhole slits and a guard slit immediately adjacent to the sample. The scattering profile was projected on a screen and imaged on to a 512 $\times$ 512 CCD camera using a macrolens. For this setup a sensitivity run was made using an isotropic scatterer (a hemispherical, silica-filled elastomer). Dark current and transmission runs and standard X-ray data correction procedures were used.[2] Typically, several sample-to-detector distances are used to expand the available range in scattering angle. Ultrasmall-angle X-ray scattering (USAXS) data was also collected for the same material to extend the range of scattering vector, $q$, to the nanometer range. USAXS data was collected at the National Institute of Standards and Technology (NIST) beam line at Brookhaven National Laboratories, X23A3 with the assistance of G. Long and D. Fischer. This instrument was used because it provides up to a decade of overlap with SALS data from our pinhole instrument.

SALS samples were run in 1-mm path-length, quartz-box spectroscopy cells filled with benzyl alcohol. Typical sample thickness were about 0.5 mm. Samples were carefully checked for multiple scattering by observation of the projected main beam. USAXS samples were run in air and were of similar thickness.

## RESULTS/DISCUSSION

SEM, Figure 1(a), and optical micrographs, Figure 1(b), of GMF samples typically display a structure analogous to models for linear polymers with extremely long, cylindrical fibers forming a continuous walk in 3D space. Figure 1(a) is an SEM micrograph from a dry fiber mat coated with gold. Figure 1(b) is an optical micrograph of the same fiber mat immersed in benzyl alcohol, which is close to index matching. The conditions of Figure 1(b) match those used for the SALS measurements. Micrographs taken at several magnifications in the regime between the overall fiber size and the fiber diameter have similar features to that of Figure 1(b), supporting a mass-fractal scaling regime, i.e., there is qualitative microscopic support for self-similarity. Further support for this scaling regime comes from SALS data, shown in Figure 2.

Figure 2 shows a typical SALS/USAXS pattern from a sample of GMF immersed in benzyl alcohol. The incident beam is perpendicular to a thin sheet of GMF. SALS intensity has been scaled to match the overlapping region between SALS and USAXS. USAXS data is measured in absolute intensity units. The combined SALS and USAXS data, shown in Figure 2 in a log(intensity) vs. log(scattering vector) plot, displays two prominent scaling regimes. Between $q = 10^1$ and $10^3$ $\mu m^{-1}$ the data is well described by Porod's law for smooth sharp interfaces,[13] $I(q) = N\,2\pi\,\Delta\rho^2\,S/V\,q^{-4} = 32\,G_1/(KD^3)\,q^{-4}$. Through use of the Porod invariant,[1–3,13,14] $Q = \int I(q)\,q^2\,dq$, the data can be normalized internally to generate the surface to volume ratio, $S/V$, for the fibers. $S/V$ can then be divided by the fiber density, for silica fibers about 2.2 g/cm$^3$, to yield the specific surface area for the fibers, 2.3 m$^2$/g in this case. At lower $q$, a weaker power-law scaling regime is observed with a slope close to $-5/3$. Although a number of structures could account for this low-dimensional scaling regime, combination of the observation of this power-law regime with the micrographs and a knowledge of the polymer scaling theory lend support to this regime reflecting a fiber self-avoiding walk, as would be seen for a polymer coil in a good solvent. Such a scaling regime describes the most random arrangement of fibers that maintain self-avoidance.

The power-law regimes of Figure 2 display two knee-like power-law limiting features that yield two radii of gyration from eq. (1). At lowest $q$ the knee in the scattering curve reflects the average overall coil size, as measured by the number of Kuhn segments in the coil, $z = 880 \pm 2$, and at intermediate $q$, the knee like feature is associated with the fiber diameter, $D = 0.79 \pm 0.01$ $\mu$m, and Kuhn step length, $K = 3.43 \pm 0.001$ $\mu$m as discussed above. The extended length (primitive path, $P$) for the fiber is, $P = zK = 3.0 \pm 0.01$ mm. These values agree with the expected values obtained by optical and electron microscopy. Er-


(a)

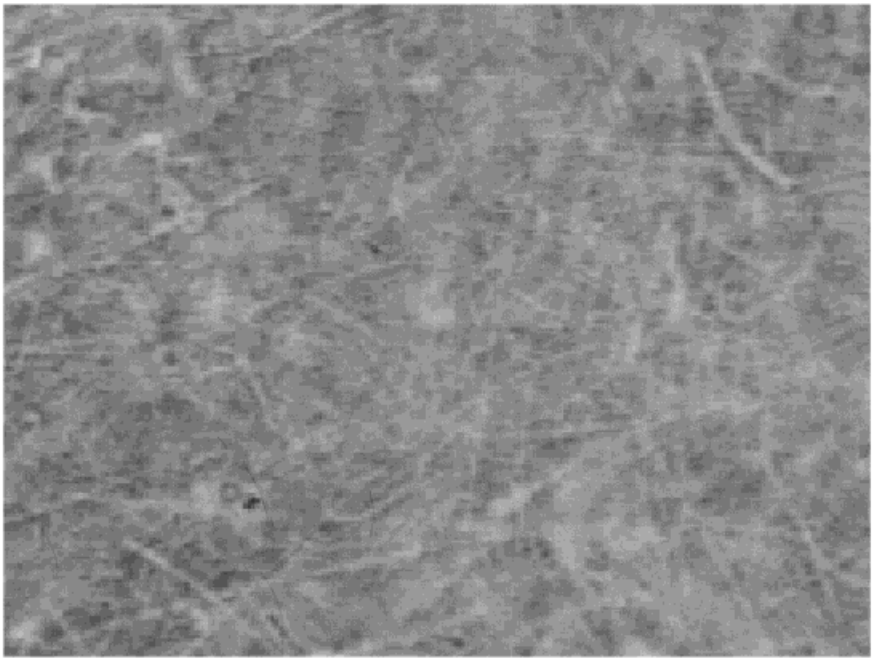

(b)

**Figure 1.** Micrographs of GMF sample showing micron-scale silica glass fibers in a polymer-like mat. (a) SEM micrograph after gold coating. This size scale corresponds to the persistence regime and the high-$q$ end of the scaling regime. (b) Optical micrograph at 20×. This size scale would correspond to the scaling regime of Figure 2 below.

rors are propagated through the least-squares fit from the statistical error in the data. The fit values represent a statistical average over the irradiated part of the sample. The statistical errors are probably narrower than the distribution in the sample, so have limited value other than to

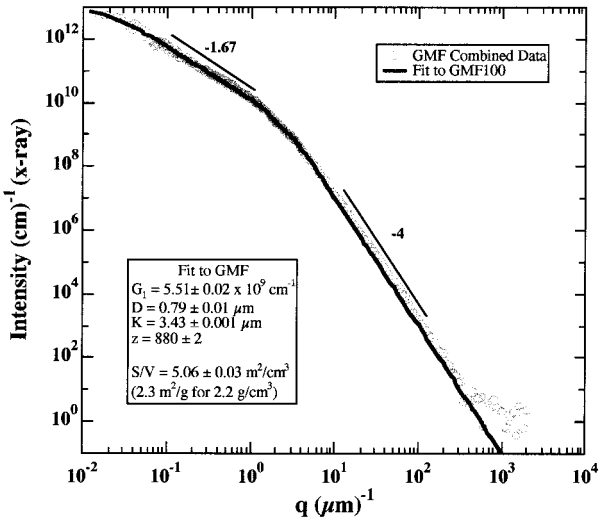


**Figure 2.** Log I vs. log $q$ plot for GMF with an incident beam normal to the sample plane. Scaling regime at low-$q$ follows good solvent scaling. High-$q$ scaling follows Porod's law. Fit uses the unified equation with four free parameters and a model based on a polymer-like structure.

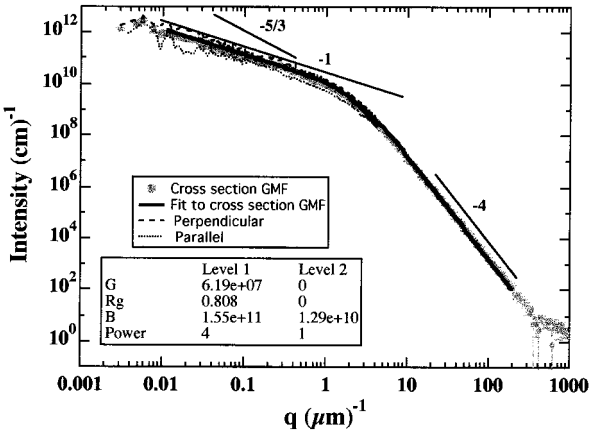


**Figure 4.** Azimuthally averaged data for GMF in cross-section.

indicate that the unified fit matches the scattering data closely.

Disordered fibrous materials are generally produced in the form of sheets. Within the plane of the sample the fibers are sometimes oriented randomly or close to randomly as in GMF. In most cases, fibers are not expected to be randomly arranged in the sheet normal direction. This is clearly the case for GMF, as can be observed microscopically or in SALS. Figure 3 shows 2D SALS patterns for GMF in cross-section and in-plane for the GMF sheet. The cross-sectional pattern shows a marked degree of anisotropy. If this anisotropic data is azimuthally averaged (averaged circularly about the beam center as a function of angle from the center) the scattering pattern of Figure 4 results. Figure 4 shows both USAXS as well as SALS data for this cross-sectional sample. In the cross-section, the scaling regime displays a slope of $-1$, indicating largely linear fibers. Sector averages of the data in Figure 3(a) shows a similar scaling regime (also shown in Fig. 4), although somewhat limited in extent at low $q$ for one of the two orientations.

The data of Figure 4, cross-sectional data, show a striking difference in terms of scaling when compared with that of Figure 2, in-plane data, as indicated by the disagreement between the line of slope $-5/3$ in Figure 4 and the data. The fiber coils, which appeared to be random with self-avoidance in the plane of the sheet, are better

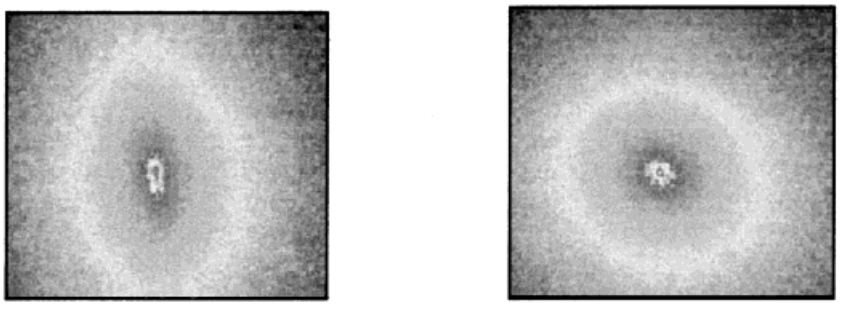


**Figure 3.** 2D orientation of GMF in cross-section and in normal to the plane of a sheet.

described as extended rods in the sheet cross-section. This means that the presumption of three-dimensional, self-avoiding-walk scaling must be modified to an apparent two-dimensional morphology, which mimics a 3D self-avoiding walk in the plane of the sheet. Variation in the apparent good-solvent scaling regime for GMF in the plane of the sheet can also be attained by deformation of the GMF fibers using a pair of tweezers (not shown).

The orientation of the cross-section sample of Figures 3 and 4 can be considered in terms of the Hermans orientation function, $f$. This is a uniaxial, dipole orientation function for the second moment of a Legendre expansion of orientation,[8] and represents a simplified view of the 3D orientation present in the sample. However, the Hermans orientation function can be a powerful approximation that can give simple information concerning the relationship between orientation and morphology. It is possible to calculate $f(q)$ for an arbitrary range of $q$, $\Delta q$, using the standard function,[8]

$$f(q) = \frac{3\langle \cos^2 \phi \rangle - 1}{2} \tag{2}$$

where,

$$\langle \cos^2 \phi \rangle = \frac{\int_0^{\pi/2} I(q, \phi) \cos^2 \phi \sin \phi \, d\phi}{\int_0^{\pi/2} I(q, \phi) \sin \phi \, d\phi} \tag{3}$$

and $\phi$ is the azimuthal angle, such as in Figure 3 (the angle around the beam center), with $\phi = 0$ being associated with the maximum in scattering intensity. This approach differs from the traditional use of the orientation function, typically in XRD for a given crystalline reflection.[8,15] Here, the purpose of the orientation function is to associate arbitrary structural features seen in SALS with size scales, roughly $d \approx 2\pi/q$, of enhanced orientation. Figure 5 shows the result of such a calculation based on the data of Figure 3 compared with the SALS data of Figure 4.

The maximum in orientation for the GMF cross-section data occurs at close to the low $q$ scaling limit for the parallel data (triangles in Fig. 5), i.e., the limit of the $-1$ slope power-law in Figures 4 and 5 for the pattern parallel to the sheet surface. The parallel pattern reflects structure normal to the sheet surface. The association of a maximum in orientation with the limitation of fiber linearity normal to the surface of the sheet supports the idea that cross-sectional orientation is a result of fiber confinement in the sheet normal direction. A similar orientation calculation with the beam normal to the sheet surface, Fig. 3, shows little orientation and no $q$ dependence to uniaxial orientation.

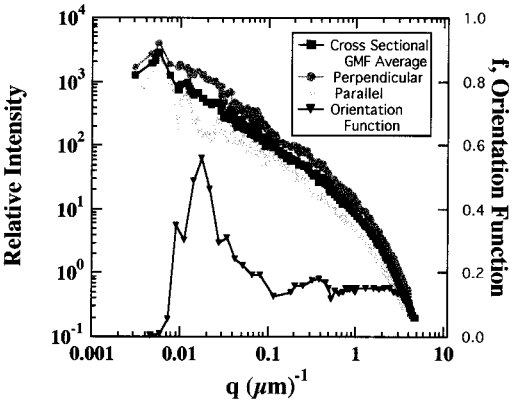


**Figure 5.** Orientation function and SALS data for GMF in cross-section as a function of $q$. Perpendicular and parallel are with respect to the plane of the mat.

A scaling approach to fiber morphology can be used to predict some physical properties for these materials. Materials such as GMF are sometimes used as absorbents, and the traditional measure of their absorption capability is made using capillary porosimetry.[16] The capillary absorption experiment involves measurement of the rate of absorption of an imbibing fluid such as water in a dipping experiment where transport is parallel to the sheet surface. The Laplace equation is used with measures of the fiber surface tension to calculate the cumulative pore volume vs. pore size. In samples with morphological asymmetry, it is the in-plane morphology that will largely govern the rate of absorption if the sample is dipped at the edge of the sheet, as is normally done in the capillary absorption experiment. To calculate the cumulative pore volume vs. pore size curve, a relationship between morphological features based on a mass-fractal model and the pore-size distribution must be determined. Recently, cumulative pore volume vs. pore-size data has been used to estimate the mass-fractal dimension of chromatographic gels.[17] Equation (4) gives the cumulative pore volume as a function of pore size for a mass-fractal structure,

$$V_p(l) = V_{\max}\left[1 - \frac{1 - (V_{\min}/V_{\max})}{1 + \exp([3 - d_f][\ln(l) - \ln(\bar{l}_{\text{pore}})]}\right] \tag{4}$$

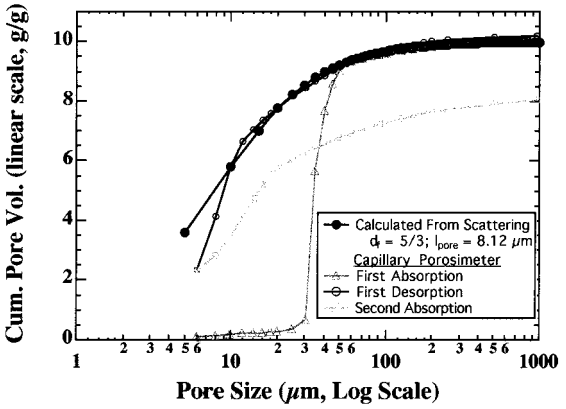


**Figure 6.** Cumulative pore volume vs. pore size from SALS and from capillary porosimetry.

This approach can be directly adapted to the inverse problem of calculating the cumulative pore volume curve from SALS data for the in-plane direction. The approach relies on four parameters, a mean pore size, maximum pore size, minimum pore size, and a mass-fractal scaling dimension. The mean pore size can be associated with the mean pore chord length from the Porod regime of the scattering curve,[13] $l_{\text{mean pore}} = 4Q/(\pi\phi_{\text{solid}}B_{\text{Porod}})$, where $Q$ is the Porod invariant discussed above, $B$ is the Porod Power-law prefactor, and $\phi_{\text{solid}}$ is the volume fraction of fiber in the sample. For the GMF sample of Figure 2 the mean pore size is about 8.12 microns. $V_{\max}$ and $V_{\min}$ are calculated for spheres of size relating to the coil $R_g$ and the fiber diameter.

The results of such a calculation are shown in Figure 6. For the capillary absorption experiment, the first desorption is usually used as a measure of the true cumulative pore volume for the sample. The first desorption shows good agreement with the cumulative pore volume calculated from the in-plane scattering pattern of GMF.

## CONCLUSIONS

Some disordered fiber mats provide an interesting analogy with thermally equilibrated, nanometer-scale polymers in that they display a well-defined scaling regime, and analogues to a coil radius of gyration and persistence unit. In this article it was shown that polymer models for these disordered micron-scale structures can be used to predict some properties of these systems. The adoption of fractal scaling laws and their theoretical basis in terms of excluded volume provides a fascinating framework within which these disordered materials can be physically described.

Disordered fiber mats, when produced as sheets, are generally anisotropic, which leads to asymmetry in the scattering patterns for cross-sectional samples. This asymmetry can be quantified through adoption of the Hermans orientation function to these systems, leading to a correlation between structural features and orientation. Scaling of GMF fibers is found to be close to that of a self-avoiding walk when viewed normal to the sheet and close to that of extended chains when viewed in cross-section. This result from SALS agrees with evidence from optical microscopy. For properties that depend on the in-plane structure, such as capillary absorption, the fractal features of scattering can be used to generate a morphological basis for physical properties of interest. Scattering features, for instance were used to calculate the cumulative pore volume distribution in GMF fiber mats with good agreement.

The use of these micron-scale disordered structures as models for nanometer-scale polymer structure is more limited. Disordered fiber mats are not at thermal equilibrium; hence, they cannot display a number of features common to nanoscale polymers such as screening effects and thermal changes in solvation. However, as simple models for certain targeted features disordered fiber mats may prove quite useful. For instance, the micrographs of Figure 1 are different than the common cartoons of "disordered," good-solvent polymer structure. This might serve as a reminder that a truely disorder structure displays some, random, correlations. The orientation of disordered fiber mats, when processed under certain conditions, may be analogous to the orientation of polymers, in thin films for instance, where the film thickness is less than the coil size. Finally, mechanical deformation of these fiber mats, which can be performed with tweezers under an optical microscope, could provide insight into some of the most basic features of linear polymer deformation under shear or elongational flow. Careful consideration of these simple systems, keeping the limitations in mind, could prove useful in the development of realistic models for nano-scale deformation of polymer coils.

This work was partially supported by the American Chemical Society through the Petroleum Research Fund Grant 30781-G7.

## REFERENCES


1. J. S. Higgins and H. C. Benoit, *Polymers and Neutron Scattering,* Oxford Science Publications: Oxford, UK, 1994.
2. G. D. Wignall, in *Physical Properties of Polymers Handbook,* J. E. Mark, Ed., American Institute of Physics Press, New York, 1996.
3. L. A. Feigin and D. I. Svergun, *Structure Analysis by Small-Angle X-ray and Neutron Scattering,* Plenum Press, New York, 1987.
4. G. Strobl, *The Physics of Polymers,* Springer Verlag, Berlin, 1996.
5. M. Doi and S. F. Edwards, *The Theory of Polymer Dynamics,* Oxford Science Publications, Clarendon Press, New York, 1986.
6. P. Degennes, *Scaling Concepts in Polymer Physics,* Cornell University Press, Ithaca, NY, 1979.
7. P. J. Flory, *Principles of Polymer Chemistry,* Cornell University Press, Ithaca, NY, 1953.
8. See, for example: G. Wilkes, *Adv. Polym. Sci.,* **8,** 91 (1971).
9. G. Beaucage, *J. Appl. Crystallogr.,* **28,** 717 (1995).
10. G. Beaucage and D. W. Schaefer, *J. Non-Cryst. Solids,* **172–174,** 797 (1994).
11. G. Beaucage, *J. Appl. Crystallogr.,* **29,** 134 (1996).
12. G. Beaucage, S. Rane, S. Sukumaran, M. M. Satkowski, L. A. Schechtman, and Y. Doi, *Macromolecules,* **30,** 4158 (1997).
13. A. Guinier and G. Fournet, *Small-Angle Scattering of X-rays,* John Wiley & Sons, New York, 1955.
14. See, for example: D. W. Schaefer, R. K. Brow, B. J. Ollivier, T. Rieker, G. Beaucage, L. Hrubesh, and J. S. Lin, in *Modern Aspects of Small-Angle Scattering,* H. Brumberger, Ed., Kluwer, Amsterdam, 1994, p. 299.
15. L. E. Alexander, *X-ray Diffraction Methods in Polymer Science,* Krieger Publishing, Malabar, FL, 1985.
16. A. W. Adamson, *Physical Chemistry of Surfaces,* Wiley–Interscience, New York, 1967.
17. M. Sernetz, H. R. Bittner, H. Willems, and C. Baumhoer, in *The Fractal Approach to Heterogeneous Chemistry, Surfaces, Colloids, Polymers,* D. Avnir, Ed., John Wiley & Sons, New York, 1989, p. 361.